



Jalalvand, M., Czél, G., & Wisnom, M. R. (2015). Damage analysis of pseudo-ductile thin-ply UD hybrid composites - A new analytical method. *Composites Part A: Applied Science and Manufacturing*, 69, 83-93. <https://doi.org/10.1016/j.compositesa.2014.11.006>

Publisher's PDF, also known as Version of record

Link to published version (if available):
[10.1016/j.compositesa.2014.11.006](https://doi.org/10.1016/j.compositesa.2014.11.006)

[Link to publication record in Explore Bristol Research](#)
PDF-document

University of Bristol - Explore Bristol Research

General rights

This document is made available in accordance with publisher policies. Please cite only the published version using the reference above. Full terms of use are available:
<http://www.bristol.ac.uk/red/research-policy/pure/user-guides/ebr-terms/>



Damage analysis of pseudo-ductile thin-ply UD hybrid composites – A new analytical method



Meisam Jalalvand^{*}, Gergely Czél, Michael R. Wisnom

Advanced Composites Centre for Innovation and Science, University of Bristol, Bristol BS8 1TR, UK

ARTICLE INFO

Article history:

Received 29 July 2014

Received in revised form 30 October 2014

Accepted 2 November 2014

Available online 8 November 2014

Keywords:

A. Hybrid

B. Fragmentation

B. Delamination

C. Analytical modelling

ABSTRACT

A new simple analytical approach for predicting all possible damage modes of Uni-Directional (UD) hybrid composites and their stress–strain response in tensile loading is proposed. To do so, the required stress level for the damage modes (fragmentation, delamination and final failure) are assessed separately. The damage process of the UD hybrid can then be predicted based on the order of the required stress for each damage mode. Using the developed analytical method, a new series of standard-thickness glass/thin-ply carbon hybrid composites was tested and a very good pseudo-ductile tensile response with 1.0% pseudo-ductile strain and no load drop until final failure was achieved. The yield stress value for the best tested layup was more than 1130 MPa. The proposed analytical method is simple, very fast to run and it gives accurate results that can be used for designing thin-ply UD hybrid laminates with the desired tensile response and for conducting further parametric studies.

© 2015 The Authors. Published by Elsevier Ltd. This is an open access article under the CC BY license (<http://creativecommons.org/licenses/by/4.0/>).

1. Introduction

Fibrous composites are strong and have a good potential for structural applications but they suffer from lack of ductility. The failure of composite materials is usually catastrophic with little or no warning. Therefore, large safety margins are applied in the design procedure, reducing the benefits of composite materials. Achieving gradual failure and pseudo ductility can help composite structures to maintain functionality even when they are overloaded, improve safety and reduce the applied safety factors.

One of the successful approaches for introducing pseudo-ductility into composite materials is hybridisation with thin plies, combining fibres with different mechanical properties to achieve a gradual failure. In a hybrid composite, the Low Strain (LS) material fails earlier but the High Strain (HS) material which has a higher failure strain can carry the load so that overall integrity is maintained [1]. If the low strain material is very thin, delamination is avoided, leading to ply fragmentation and associated pseudo-ductility. However, if the hybrid's configuration is not carefully designed, the hybrid may not only break suddenly, but also shows a lower strength than the constituents.

Fig. 1 shows schematically how the strength of a typical glass/carbon hybrid varies with different proportions of low to high

strain material [2]. Points A and D indicate the strength of the glass and carbon respectively and line BD indicates the stress in the laminate when the carbon layer starts to fail. The line AC also shows the ultimate strength of the hybrid after multiple fractures in the carbon layer. To the right of point C, the carbon layer fails prematurely at the stress level shown by CD and the glass layer cannot sustain the transferred load.

Although the model proposed by Aveston, Cooper, and Kelly [3,4] (Fig. 1) showed the effect of UD hybrid's constituents proportion for avoiding catastrophic failure, it did not consider delamination. Based on this model, if the proportion of the low to high strain material was lower than a critical value, multiple fractures would happen and if the proportion was higher than a critical value, the hybrid would fail prematurely. However, it has been shown [1,5,6] that delamination is another possible damage mode which is not included in Aveston, Cooper and Kelly's model. Other sophisticated analysis methods such as [7–9] which are based on considering the fibre strength variation also studied the effect of the proportion of low to high strain material as well as different fibre arrangements on the hybrid's strength but again, they did not take delamination into account. More recent studies on application of hybrids to avoid catastrophic failure and increase the pseudo-ductility of composite materials [10–12] have reported delamination propagating from the tips of the first crack in the low strain material.

Recently, Czél and Wisnom [13] showed that laminates with the same carbon/glass proportion may have totally different tensile

^{*} Corresponding author.

E-mail addresses: m.jalalvand@bristol.ac.uk, jalalvand.meisam@gmail.com (M. Jalalvand).

Nomenclature

α	the Young's modulus ratio of the low to high strain material	E_H	modulus of the high strain material
β	the thickness ratio of the low to high strain material	E_L	modulus of the low strain material
λ	the strength ratio of the low to high strain material	E_{int}	initial modulus of the UD hybrid laminate
δ	displacement along force direction at the end of RVE	F	applied force at the end of RVE
ϵ_{HF}	failure strain of the high strain material	$F_{L@sat}$	force in the low strain material at the saturation and in post saturation
ϵ_{LF}	failure strain of the low strain material	G	strain energy release rate
$\epsilon_{@psat}$	strain in the laminate at the post-saturation phase	G_{IIc}	mode II critical strain energy release rate
$\epsilon_{@HF-PS}$	strain in the laminate at the post-saturation phase when the high strain material fails	K_i	($i = 1, 2$ or tot) the stiffness of the relevant part in the delamination RVE model
σ	applied stress in the laminate	K_t	stress concentration factor
$\sigma_{@LF}$	laminate stress at low strain material failure	L_i	($i = 1, 2$ or tot) the length of the relevant part in the delamination RVE model
$\sigma_{@HF}$	laminate stress at high strain material failure	L	length of the hybrid specimen
$\sigma_{@Frg}$	laminate stress at low strain material fragmentation	S_H	strength of the high strain material
$\sigma_{@del}$	stress in the laminate at which delamination propagates	S_L	strength of the low strain material
$\sigma_{@psat}$	stress in the laminate at the post-saturation phase	\bar{S}_L	strength distribution average of the low strain material
σ_H	stress in the high strain material	U_{tot}	total strain energy of a RVE
$\sigma_{H,max}$	maximum stress in the high strain material	V	volume of the specimen
$\sigma_{H,eq}$	equivalent stress in the high strain material	W	width of the specimen
σ_L	stress in the low strain material	m	Weibull modulus of high strain material strength distribution
$\sigma_{L@psat}$	the post-saturated constant stress in the low strain material	t_L	half thickness of the low strain material
σ_{eq}	equivalent stress for fibre failure criterion based on Weibull random distribution	t_H	half thickness of the high strain material
D_i	is equal to $E_H t_H$ if $i = 1$ and $E_H t_H + E_L t_L$ if $i = 2$		

responses. For example, a UD sandwich hybrid with one E-Glass layer on each side and two Carbon layer in the middle, [EG/C₂/EG], fails straightaway after the first crack in the carbon layer but the final failure strain of [EG₂/C₄/EG₂] layup, with exactly the same carbon/glass proportion, is almost double, because of their difference in delamination propagation. In the latter layup, there is sudden delamination propagation after the first crack in the carbon layer, which suppresses the stress concentration in the E-glass layers. But in the former one, the carbon layer is thin so delamination cannot propagate and the stress concentration around the crack in the carbon layer breaks the glass layers. This example clearly indicates the importance of including all possible damage modes to achieve an accurate analysis.

Unlike previous studies [10–12] on introducing pseudo-ductility to composites in which delamination was assumed to be acceptable, Czél and Wisnom [13] avoided this damage mode since it is accompanied by a significant load drop and loss of integrity of the whole specimen. Their solution to avoid catastrophic delamination was to use thin-ply of carbon/epoxy by which the energy release rate due to delamination is kept low. The effect of

the proportion as well as the absolute thickness of the constituents has also been studied with a Finite Element approach [14] and it has been shown that both the proportion and absolute thickness of the constituent layers have significant influences on the tensile response of hybrid composites.

The aim of this paper is to propose a new analytical modelling approach by which, all possible UD hybrid damage modes are taken into account. This analytical method is then used for designing a new set of experimental tests. The difference between the new experimental results compared to previous ones such as [15–17] is that a very good nonlinear tensile response with a long plateau and high yield stress was achieved with no load drop before final failure. The experimental results are significantly improved compared to the previous ones [13] in terms of both pseudo-ductility and yield stress.

Compared with the FE-based method proposed in [14], the analytical method proposed in this paper is significantly faster. Since there is no pre-processing cost for finite element model preparation in the analytical approach and the solution time is negligible, the proposed method is an ideal choice for analysing different types of configuration and carrying out parametric studies that will be performed in a companion paper. The effect of geometric parameters will be assessed by introducing novel “Damage Mode Map” and material parametric studies will be performed to show the trade-off between pseudo-ductility and strength in UD hybrids. These two parametric studies will help to obtain simple, quick and accurate design guidelines for UD hybrid laminates.

1.1. Damage modes in UD hybrid composites

As discussed in [13,14], four different scenarios can occur after the first crack initiation in the low strain material:

1. Premature failure of the high strain material.
2. Catastrophic delamination followed by high strain material failure.

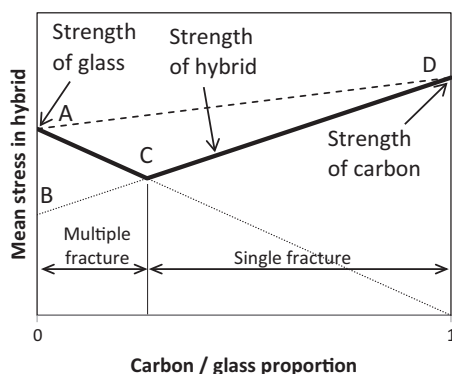


Fig. 1. Theoretical strength of glass/carbon fibre hybrid composites (adapted from [2,6]).

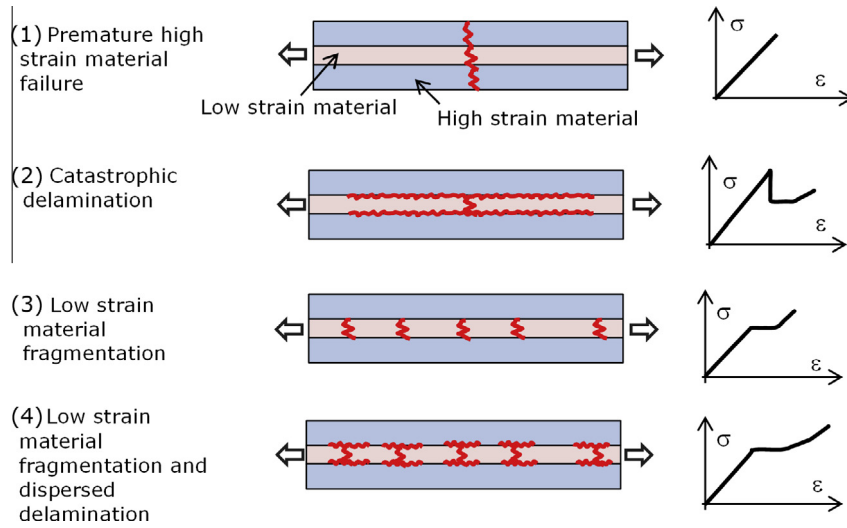


Fig. 2. Different damage scenarios of UD hybrid laminates. (For interpretation of the references to colour in this figure legend, the reader is referred to the web version of this article.)

3. Fragmentation (multiple fractures) in the low strain material and then high strain material failure.
4. Fragmentation in the low strain material followed by dispersed delamination and then high strain material failure.

These cases and their stress–strain curves are shown schematically in Fig. 2. Neither catastrophic nor dispersed delamination was considered in the analytical approach proposed in [3,4] so it is not able to predict damage scenarios number 2 and 4 or to cope with the effect of the absolute thickness of the constituents.

The first aim of this study is to propose a simple analytical approach by which, the full stress–strain response of any UD hybrid composite can be predicted. This analytical approach can be applied to study the effect of geometric parameters and material properties in the next step. Very low computational cost and the ability to capture all different combinations of damage modes have made this approach an ideal tool for parametric studies.

2. Damage modes

Since there is no stress variation within the layers along the specimen before any damage occurrence, the first instance of damage in UD hybrid composites is fibre failure in the low strain material. But depending on the material properties and the hybrid configuration, the four different damage scenarios mentioned in the introduction may occur. These damage scenarios are composed of the three different damage modes of (i) fragmentation/multiple fracture of the low strain material, (ii) delamination and (iii) failure of the high strain material. The failure of both low and high strain materials can be predicted by comparing the values of stress (σ_L and σ_H) against their tensile strength (S_L and S_H). Delamination development is also predicted when the interlaminar energy release rate becomes equal or higher than the critical energy release rate, G_{IIc} . The first failure in the low strain material and the three possible following damage modes are discussed in details in this section.

2.1. First failure in the low strain material

Before the first failure in the low strain material, there is no stress variation along the hybrid specimen and the strain field is uniform in each layer along the specimen. Therefore the first

damage instance in any UD hybrid composite is failure of the low strain material. The initial modulus of a hybrid laminate before any damage in the low strain material, E_{int} , can easily be found from Eq. (1) in which E_H and E_L are the high and low strain material modulus respectively and t_H and t_L are their half thickness as shown in Fig. 3. The modulus and thickness ratios $\alpha = \frac{E_L}{E_H}$ and $\beta = \frac{t_L}{t_H}$ are constant for each specific hybrid laminate.

$$E_{int} = \frac{E_L t_L + E_H t_H}{t_L + t_H} = E_H \frac{\alpha\beta + 1}{\beta + 1} \quad (1)$$

The stress in the laminate at which the first crack in the low strain material occurs, $\sigma_{@LF}$, depends on the failure strain of the low strain material, ϵ_{LF} , which can be related to the low strain material's strength, S_L , and modulus, E_L , as $\epsilon_{LF} = \frac{S_L}{E_L}$. According to the schematic shown in Fig. 3, laminate stress at low strain failure, $\sigma_{@LF}$, can be defined as Eq. (3).

$$\sigma_{@LF} = \frac{S_L}{E_L} \frac{E_H t_H + E_L t_L}{t_L + t_H} = S_L \frac{\alpha\beta + 1}{\alpha(\beta + 1)} \quad (2)$$

The @ sign is used to show that the stress, σ , corresponds to the appearance of a certain damage mode (low strain material failure here) within the laminate. This symbol will be used in this paper and if there is no character before @ in the subscript, the stress is related to the laminate level but characters L and H before @ in the index mean that the stress is associated with low or high strain materials. For instance, $\sigma_{@LF}$, $\sigma_{L@LF}$ and $\sigma_{H@LF}$ are stresses in the laminate, low strain material and high strain material respectively, all at the failure of the low strain material.

2.2. Fragmentation in the low strain material

After the first failure in the low strain material, different damage modes such as gradual fragmentation (multiple fractures) in the low strain material may occur. It is possible to define a *critical length* for the low strain material layer, l_c , where the stress in the low strain material is lower than the far field stress as shown in Fig. 3. Assuming an elastic–perfectly plastic shear response for the interface with the shear yield stress equal to τ_y , the critical length can be related to the strength distribution average and thickness of the low strain material layer (\bar{S}_L , t_L) with unit depth in the z direction as in Eq. (3). In an ideal low strain material with completely uniform strength distribution, the strength distribution average, \bar{S}_L , is equal to the strength, S_L , but due to the variation of

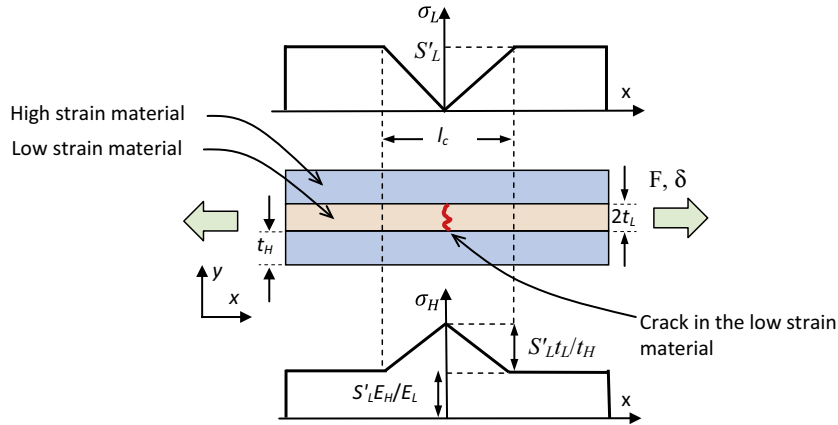


Fig. 3. The stress variation in the low and high strain materials around a crack in the low strain material. (For interpretation of the references to colour in this figure legend, the reader is referred to the web version of this article.)

strength in the fibres, the strength distribution average is always higher than the minimum apparent strength. Fig. 3 indicates the stress variation in both high and low strain material layers around a crack.

$$l_c = \frac{2\dot{S}_L t_L}{\tau_y} \quad (3)$$

The crack in the low strain material causes a stiffness reduction since the low strain material's contribution to load transfer becomes lower and as a result, the overall laminate stiffness decreases. If the damage mode does not change, any increase in the elongation of the laminate leads to more cracks in the low strain material. Since the stress within the distance of $l_c/2$ from any crack in the low strain material is lower than in other parts, the new cracks are likely to occur only in the parts with uniform low strain material stress further than $l_c/2$ distance away from existing cracks. The applied load/stress can easily be related to the stress values in the low and high strain materials where the stress stays constant along the length. Therefore, for an ideal low strain material with constant strength distribution along the length, the stress in the laminate at which fragmentation progresses, $\sigma_{@Frg}$, can be expressed as Eq. (4) which is similar to Eq. (2). This equation clearly indicates that as long as \dot{S}_L stays constant along the specimen, the applied stress is constant. In other

words, for an ideal layer with no strength variation along the length, the stress does not drop or rise during fragmentation.

$$\sigma_{@Frg} = \dot{S}_L \frac{\alpha\beta + 1}{\alpha(\beta + 1)} \quad (4)$$

The fragmentation in the low strain material becomes saturated and stops when there is no longer any part of the low strain material with constant stress. The distance between the cracks can therefore vary from l_c to $l_c/2$, as shown in Fig. 4.

The stiffness of a Representative Volume Element (RVE) with the length $l_c \geq l \geq l_c/2$ and two cracks in the low strain material on each side (Fig. 5) can be found by integrating the variation of strain in the high strain material.

The stress in the high strain material between two transverse cracks separated by an arbitrary distance l where $l_c \geq l \geq l_c/2$, can be found using Eq. (5).

$$\sigma_H(x) = \dot{S}_L \frac{E_H}{E_L} + \dot{S}_L \frac{t_L}{t_H} \left(1 - \frac{l}{l_c}\right) + \dot{S}_L \frac{t_L}{t_H} \frac{2x}{l_c} \quad 0 \leq x \leq \frac{l}{2} \quad (5)$$

The elongation of the RVE can then be found by integrating the strain over its length:

$$\delta = 2 \int_0^{l/2} \epsilon_H(x) dx = 2 \int_0^{l/2} \left[\frac{\dot{S}_L}{E_H} \left(\frac{1}{\alpha} + \beta\right) + \frac{\dot{S}_L}{E_H} \beta \frac{(2x - l)}{l_c} \right] dx \quad (6)$$

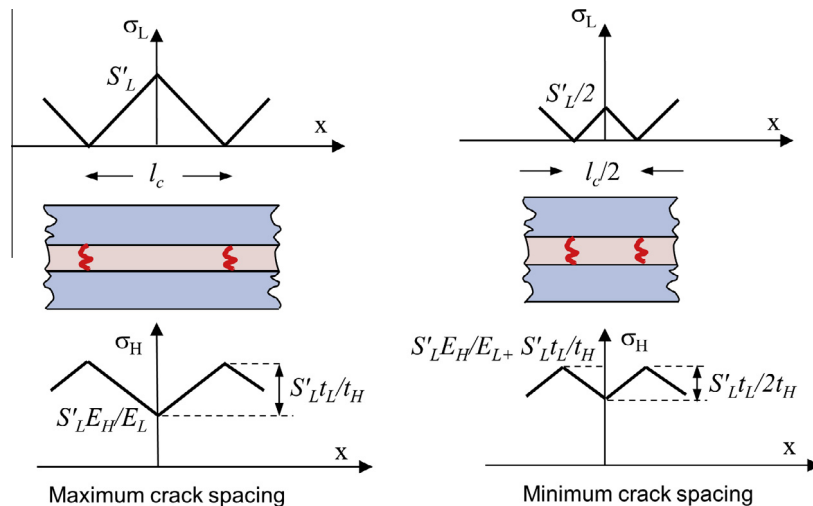


Fig. 4. Minimum and maximum crack spacing in the low strain material at saturation. (For interpretation of the references to colour in this figure legend, the reader is referred to the web version of this article.)

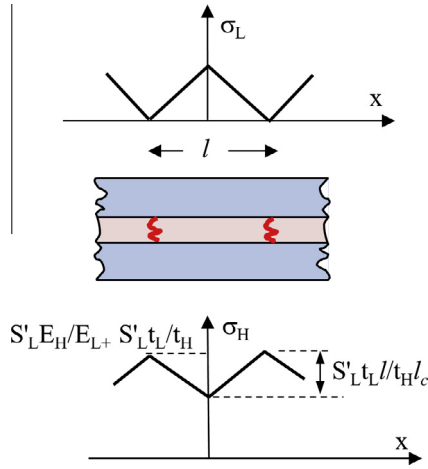


Fig. 5. A representative volume element with length of $l_c \geq l \geq l_c/2$. (For interpretation of the references to colour in this figure legend, the reader is referred to the web version of this article.)

After some manipulation, the average strain of the high strain material becomes:

$$\bar{\epsilon}_H = \frac{\delta}{l} = \frac{\dot{S}_L}{E_H} \left(\frac{1}{\alpha} + \beta \right) - \frac{\dot{S}_L \beta}{2E_H} \frac{l}{l_c} \quad (7)$$

The effective modulus of such a RVE with length $l_c \geq l \geq l_c/2$ then can be found as:

$$E_{RVE}(l) = \frac{\sigma_{@Frag}}{\bar{\epsilon}_H} = \frac{E_H(1 + \alpha\beta)}{(1 + \beta) \left(1 + \beta\alpha - \frac{l}{2l_c} \alpha\beta \right)} \text{ where } \frac{l_c}{2} \leq l \leq l_c \quad (8)$$

The overall modulus of a long saturated specimen with n cracks in the low strain material, E_{sat} , can be related to the modulus of the RVEs within the laminate by Eq. (9) where l_{tot} is the full length of the specimen.

$$\frac{l_{tot}}{E_{sat}} = \frac{l_1}{E_{RVE-1}} + \frac{l_2}{E_{RVE-2}} + \frac{l_3}{E_{RVE-3}} + \dots + \frac{l_n}{E_{RVE-n}} = \sum_{i=1}^n \frac{l_i}{E_{RVE-i}} \quad (9)$$

For a large number of cracks ($n \gg 1$) and after substituting Eq. (8) into (9):

$$\frac{l_{tot}}{E_{sat}} = \sum_{i=1}^{n \gg 1} l_i \left(\frac{1 + \beta}{E_H} - A l_i \right) \text{ where } A = \frac{\beta\alpha(1 + \beta)}{2E_H l_c (1 + \alpha\beta)} \quad (10)$$

Constant A is just for easier manipulation of the relations. The compliance of the laminate with saturated fragmentation can be found from the following equation, taking into account that $l_{tot} = \sum_{i=1}^n l_i$.

$$\frac{1}{E_{sat}} = \frac{1 + \beta}{E_H} \frac{\sum_{i=1}^{n \gg 1} l_i}{l_{tot}} - A \frac{\sum_{i=1}^{n \gg 1} l_i^2}{l_{tot}} = \frac{1 + \beta}{E_H} - A \frac{\sum_{i=1}^{n \gg 1} l_i^2}{l_{tot}} \quad (11)$$

We know that the variable l_i changes from $l_c/2$ to l_c randomly. Therefore l_i can be defined by a random distribution as follows:

$$l_i = \frac{l_c}{2} (1 + \eta_i) \quad (12)$$

where η_i is a random variable between 0 and 1 for the i th crack distance. Substituting Eq. (12) and $l_{tot} = \sum_{i=1}^n l_i$ into Eq. (11) leads to:

$$\frac{1}{E_{sat}} = \frac{1 + \beta}{E_H} - A \frac{l_c}{2} \frac{\sum_{i=1}^n (1 + 2\eta_i + \eta_i^2)}{\sum_{i=1}^n (1 + \eta_i)} \quad (13)$$

Assuming that the probability of having different crack spacing in the saturated condition is similar, the probability density function of different values of the assumed random variable η_i becomes as Eq. (14).

$$f(x) = \begin{cases} 1 & 0 \leq x \leq 1 \\ 0 & x < 0 \text{ or } x > 1 \end{cases} \quad (14)$$

For large values of n , the result of the summations in the numerator and denominator of the fraction (13) can be related to the expected value and the total number n :

$$\begin{aligned} \sum_{i=1}^n 1 &= n \int_{-\infty}^{+\infty} f(x) dx = n \\ \sum_{i=1}^n \eta_i &= n \int_{-\infty}^{+\infty} x f(x) dx = \frac{n}{2} \\ \sum_{i=1}^n \eta_i^2 &= n \int_{-\infty}^{+\infty} x^2 f(x) dx = \frac{n}{3} \end{aligned} \quad (15)$$

Substituting the results from Eq. (15) into Eq. (13) becomes:

$$\frac{1}{E_{sat}} = \frac{1}{E_H} \left(1 + \beta - \frac{7}{18} \frac{\alpha\beta(1 + \beta)}{(1 + \alpha\beta)} \right) \quad (16)$$

And finally, the modulus of the laminate with randomly saturated fragmentation in the low strain material becomes as follows:

$$E_{sat} = E_H \frac{1 + \alpha\beta}{(1 + \beta) \left(1 + \frac{11}{18} \alpha\beta \right)} \quad (17)$$

The result of Eq. (17) interestingly shows that the modulus of a laminate with saturated low material fragmentation is related only to the ratios of moduli (α) and thicknesses (β) and is independent of the critical length of the layer and the shear strength of the interface. The only difference between the initial and saturation moduli (E_{int} and E_{sat} in Eqs. (1) and (17)) is the expression $(1 + \frac{11}{18} \alpha\beta)$ in the denominator of (17). To increase the difference between values of initial and saturation moduli, the low strain material should be as thick and stiff as possible for a selected high strain material.

When the laminate is completely saturated by cracks in the low strain material, no more cracking can happen in the low strain material. Since an elastic-completely plastic behaviour has been assumed for the interface, the contribution of the low strain material in load transfer stays constant, regardless of the value of strain up to the next damage mode. The force in the low strain material at the saturation state, $F_{L@sat}$, can be found by subtracting the load carried by the high strain layer from the overall force in the laminate at the saturation point:

$$F_{L@sat} = \sigma_{Frag}(t_L + t_H) - \frac{\sigma_{Frag}}{E_{sat}} E_H t_H = \sigma_{Frag} \left((t_L + t_H) - \frac{E_H}{E_{sat}} t_H \right) \quad (18)$$

The post-saturated stress in the low strain material, $\sigma_{L@psat}$, can be found by substituting Eqs. (17) into (18) as below.

$$\sigma_{L@psat} = \frac{F_{L@sat}}{t_L} = \frac{\sigma_{Frag}}{t_L} \left((t_L + t_H) - \frac{E_H}{E_{sat}} t_H \right) = \frac{7}{18} \dot{S}_L \quad (19)$$

The final result of Eq. (19) shows that the average stress after the saturation phase of the low strain material is only a function of the average strength distribution of the low strain material. Therefore, the stress-strain relation after fragmentation saturation, $\sigma_{@psat}$ and $\epsilon_{@psat}$ respectively, becomes:

$$\sigma_{@psat} = \frac{E_H \epsilon_{@psat} t_H + \sigma_{L@psat} t_L}{t_H + t_L} = \frac{E_H}{1 + \beta} \epsilon_{@psat} + \frac{7}{18} \dot{S}_L \frac{\beta}{1 + \beta} \quad (20)$$

2.3. Delamination propagation

Fig. 6 indicates a quarter of a $2L$ long hybrid specimen including a crack in the low strain material at the middle and also an inter-laminar crack. This part is a Representative Volume Element (RVE) of the whole specimen. Since the delaminated part of the low strain material does not contribute to load transfer, it is not shown in this figure. The length of the delaminated and un-delaminated

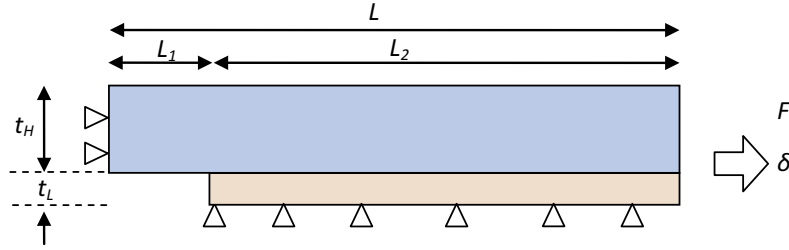


Fig. 6. Representative Volume Element (RVE) of a UD hybrid to predict delamination. (For interpretation of the references to colour in this figure legend, the reader is referred to the web version of this article.)

parts is equal to L_1 and L_2 respectively and t_H and t_L are half of the total thickness of the high and low strain material in the hybrid.

The stiffness of the RVE, K_{tot} , depends on the length of the delamination and the stiffness of delaminated and un-delaminated parts, K_1 and K_2 . The relationship between the stiffness of these parts and the elastic modulus of the high and low strain material and their thickness can be written as the following equations.

$$K_1 = \frac{E_H t_H}{L_1} = \frac{D_1}{L_1} \text{ and } K_2 = \frac{E_H t_H + E_L t_L}{L_2} = \frac{D_2}{L_2} \quad (21)$$

where D_1 and D_2 are used for easier manipulation of the equations. The total stiffness of the RVE can be found as follows:

$$\frac{1}{K_{tot}} = \frac{1}{K_1} + \frac{1}{K_2} \Rightarrow K_{tot} = \frac{D_1 D_2}{D_1 L_2 + D_2 L_1} \quad (22)$$

The overall strain energy of the RVE under applied force F and displacement δ becomes:

$$U_{tot} = \frac{1}{2} F \delta = \frac{1}{2} K_{tot} \delta^2 = \frac{1}{2} \frac{D_1 D_2}{D_1 L_2 + D_2 L_1} \delta^2 \quad (23)$$

Considering an infinitesimal crack length increment of δL_1 , the energy release rate in constant displacement becomes:

$$G = -\frac{\partial U_{tot}}{\partial L_1} = -\frac{1}{2} D_1 D_2 \delta^2 \frac{\partial \left(\frac{1}{D_1 L_2 + D_2 L_1} \right)}{\partial L_1} = \frac{D_1 D_2 \delta^2}{2} \frac{D_2 - D_1}{(D_1 L_2 + D_2 L_1)^2} \quad (24)$$

This shows that for a certain RVE length, the energy release rate is a function of the applied displacement and also the delaminated length. According to fracture mechanics, the interlaminar crack propagates when the energy release rate becomes equal to the critical energy release rate, $G_{II} = G_{IIc}$. So the applied displacement for crack propagation at an interface with G_{IIc} toughness can be found as follows:

$$\delta = \sqrt{\frac{2G_{IIc} (D_1 L_2 + D_2 L_1)^2}{D_1 D_2 (D_2 - D_1)}} \quad (25)$$

Then the stiffness of the RVE $G_{II} = G_{IIc}$ when can be found from Eq. (26):

$$K_{tot} = \frac{D_1 D_2}{\delta \sqrt{\frac{D_1 D_2}{2} \frac{D_2 - D_1}{G_{IIc}}}} \quad (26)$$

Using Eqs. (22), (25) and (26), it is possible to find the stress level at which delamination development occurs, (which will be referred to hereafter as the delamination stress, σ_{del}):

$$\sigma_{\text{del}} = \frac{F}{t_H + t_L} = \frac{1}{t_H + t_L} \sqrt{\frac{2G_{IIc} D_1 D_2}{D_2 - D_1}} = \sqrt{\frac{2G_{IIc} E_H}{t_H}} \frac{1}{1 + \beta} \sqrt{\frac{1 + \alpha \beta}{\alpha \beta}} \quad (27)$$

According to Eq. (27), while a crack is stably propagating, the applied stress is independent of crack length and therefore stays

constant. If the applied stress to a RVE is lower than the delamination stress, no crack propagation is expected but if the applied load becomes equal to or greater than the delamination stress, the crack starts to propagate until the stress level reduces to below σ_{del} . Eq. (28) shows the crack propagation criterion where σ is the stress applied to the laminate.

$$\begin{cases} \sigma < \sigma_{\text{del}} & \text{No crack propagation} \\ \sigma \geq \sigma_{\text{del}} & \text{crack propagation} \end{cases} \quad (28)$$

2.4. Failure of the high strain material

The RVE shown in Fig. 6 can also be used for failure analysis of the high strain material. The simplest failure criterion is to compare the highest stress in the high strain material with its strength, S_H . Since the low strain material is not contributing to load transfer, the stress in part 1 of the high strain material is higher than in part 2. If a stress concentration factor of K_t is assumed around the interlaminar crack tip, the maximum/critical value of longitudinal stress in the high strain material becomes as in Eq. (29), where σ is the stress in the laminate.

$$\sigma_{H_max} = K_t (1 + \beta) \sigma \quad (29)$$

During low strain material fragmentation, the stress level in the laminate remains constant but the volume of the high strain material under higher stresses increases. To take the size effect into account, an equivalent stress (σ_{eq}) is calculated for the high strain material corresponding to uniform tensile stress in unit volume. Based on the Weibull random distribution proposed for fibre failure [18], it is possible to define an equivalent stress as in Eq. (30) where m is the Weibull modulus, $\sigma_1(x)$ is the distribution of stress in the fibre direction as a function of x location, and V is the whole high strain material volume.

$$\sigma_{eq} = \sqrt[m]{\int_V (\sigma_1(x))^m dV} \quad (30)$$

Therefore, the equivalent stress for the cases of complete delamination or saturated fragmentation in the low strain material can be related to the maximum stress in the laminate as follows:

$$\sigma_{H_eq} = \sigma_{H_max} \sqrt[m]{V} = K_t (1 + \beta) \sigma \sqrt[m]{V} \quad (31)$$

High strain material failure can be checked by comparing the equivalent stress against its characteristic strength for unit volume, $\sigma_{H_eq} = S_H$. Therefore, the stress in the laminate when the high strain material fails, σ_{HF} , can be found as follows:

$$\sigma_{\text{HF}} = \frac{S_H}{K_t} \frac{1}{\sqrt[m]{V(1 + \beta)}} \quad (32)$$

It is worth mentioning that Eq. (31) is an approximation of the equivalent stress if delamination does not initiate because the stress distribution is not uniform along the fibre direction in a hybrid with saturated fragmentation. To have a more accurate

equivalent stress for high strain material failure after fragmentation saturation, the stress distribution given in Eq. (5) should be substituted in (30). This operation leads to a nonlinear integral equation that can be solved for example by trial and error. For a typical hybrid case, this method was used and the final failure stress of the high strain material was less than 2% higher than the result of Eq. (32). Since this difference is not significant, Eq. (32) is used in the rest of this paper for post-fragmentation saturation situations.

3. Stress–strain response

In the previous section, three criteria for the damage modes of (i) fragmentation in the low strain material, (ii) delamination and (iii) failure in the high strain material were studied. Table 1 summarises the three stress levels at which these damage modes are expected to occur.

At the first step of finding the stress–strain curve of a UD hybrid composite, the required stress for each of the possible damage modes needs to be found using Table 1. The expected damage process depends on the order of the required stress for the damage modes. The procedure for finding the damage process is shown in Fig. 7. Firstly the stresses at which the low and high strain materials fail are compared and then the stress at which delamination propagates is considered. After the order of the

failure stresses is found, it is possible to draw the stress–strain curve. Fig. 8 indicates the stress–strain responses of all four possible damage processes of UD hybrid composites.

If the stress for high strain material failure is lower than the other two damage modes, the laminate fails prematurely right after the first low strain material failure (first case in Fig. 8). But the stress–strain response exhibits some nonlinearity due to other damage modes developing before final failure if the required stress for the other damage modes is lower than that of the high strain material. If the value of the required stress for delamination is lower than for the other two damage modes, catastrophic delamination propagates after first failure of the low strain material straightaway (second case in Fig. 8). Gradual failure can be achieved only when the required stress for the low strain material fragmentation is lower than the other two damage modes (third and fourth cases in Fig. 8).

After determination of the damage process for a particular hybrid laminate, it is possible to draw the stress–strain response using the characteristic points given in Table 2, connected by straight lines from the origin up to high strain material failure.

All of the characteristic points required for drawing the stress–strain responses of UD hybrid composites have been discussed earlier except the final failure strain of the third case in Fig. 8, $\epsilon_{@HF-PS}$ where PS stands for Post-Saturation situation. To find the strain value at which the high strain material fails after fragmentation saturation of the low strain material, it is only necessary to substitute the high strain material failure stress ($\sigma_{@HF}$) in the left hand side of Eq. (20). Therefore, the strain at which the high strain material fails after fragmentation saturation of the low strain material is found from Eq. (33). The first term in this equation is the high strain material failure strain in the second and fourth cases shown in Fig. 8 and the second term shows the amount of strain reduction due to the load carried by the low strain material.

$$\epsilon_{@HF-PS} = \frac{\epsilon_{FH}}{K_t \sqrt[m]{V}} - \frac{7 \dot{\epsilon}_L \beta}{18 E_H} \quad (33)$$

Table 1
Summary of the stress in the laminate for each damage mode.

Damage mode	Equation No.	Equation
Fragmentation in the low strain material	(4)	$\sigma_{@LF} = \dot{\epsilon}_L \frac{\alpha\beta + 1}{\alpha(\beta + 1)}$
Delamination	(27)	$\sigma_{@del} = \frac{1}{1 + \beta} \sqrt{\frac{1 + \alpha\beta 2G_{IIC}E_H}{\alpha\beta t_H}}$
Failure in the high strain material	(32)	$\sigma_{@HF} = \frac{S_H}{K_t} \frac{1}{(1 + \beta)^{\frac{m}{\sqrt{V}}}}$

HSM: High Strain Material

LSM: Low Strain Material

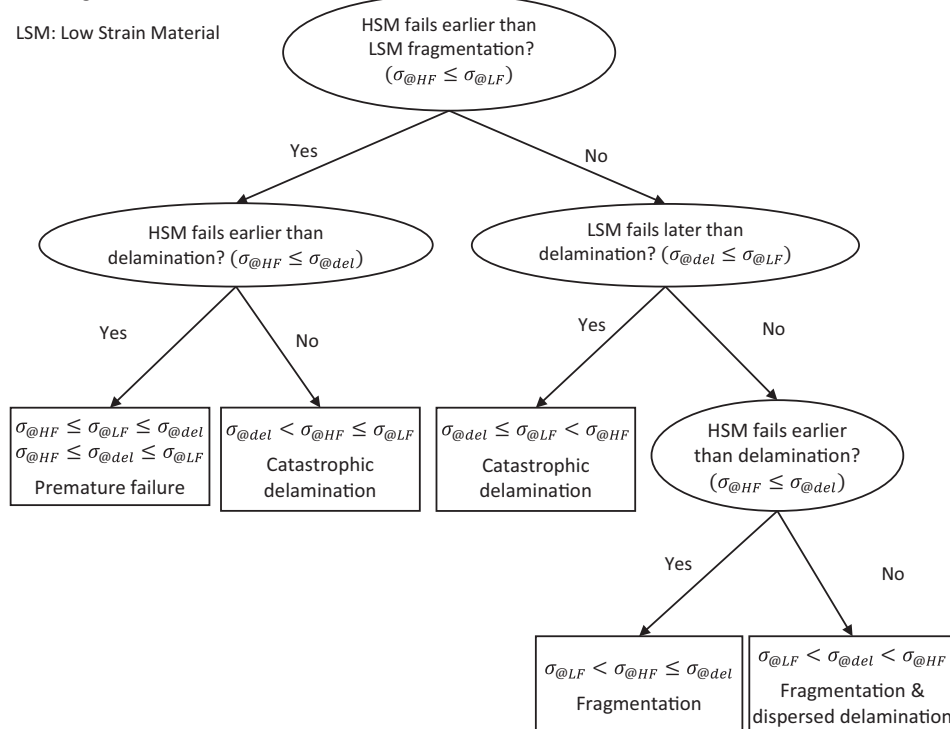


Fig. 7. The procedure for finding the hybrid's damage process based on the order of required stresses for each damage mode.

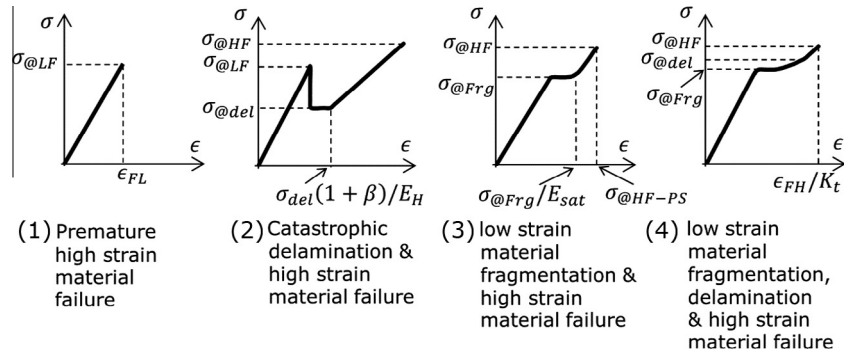


Fig. 8. Stress-strain response of four possible damage scenarios in UD hybrids.

Table 2

Coordinates of characteristic points of different damage processes on stress-strain graph.

	Point 1	Point 2	Point 3	Point 4	Point 5
Premature high strain material failure	(0,0)	$(\epsilon_{FL}, \sigma_{@LF})$			
Catastrophic delamination & high strain material failure	(0,0)	$(\epsilon_{FL}, \sigma_{@LF})$	$(\epsilon_{FL}, \sigma_{@del})$	$(\frac{\sigma_{del}}{E_{int}}, \sigma_{@del})$	$(\frac{\epsilon_{FH}}{K_t \sqrt[3]{V}}, \sigma_{@HF})$
Low strain material fragmentation & high strain material failure	(0,0)	$(\epsilon_{FL}, \sigma_{@LF})$	$(\frac{\sigma_{@Frg}}{E_{sat}}, \sigma_{@Frg})$	$(\epsilon_{@HF-PS}, \sigma_{@HF})$	
Low strain material fragmentation, delamination & high strain material failure	(0,0)	$(\epsilon_{FL}, \sigma_{@LF})$	$(\frac{\sigma_{@Frg}}{E_{sat}}, \sigma_{@Frg})$	$(\frac{\sigma_{del}}{E_{int}}, \sigma_{@del})$	$(\frac{\epsilon_{FH}}{K_t \sqrt[3]{V}}, \sigma_{@HF})$

4. Experimental pseudo-ductile response

In this part, the analysis results of different hybrid configurations made from two different glass epoxy/carbon epoxy hybrid combinations are compared against experimental results. The first set of materials, E-glass epoxy/TR30 high strength carbon epoxy hybrid, has been experimentally studied [13] with the layups of $[EG/C_m/EG]$ ($m = 1, 2$) and $[EG_2/C_n/EG_2]$ ($n = 1-4$) where EG and C stand for the UD 0.125 mm standard-thickness E-Glass and thin Carbon prepreg layers with 30 μ m thickness respectively whereas m and n indicate the number of carbon layers.

In this test series, the $[EG_2/C_2/EG_2]$ layup showed a pseudo-ductile tensile response without any load drop before the final failure. However, the E-glass layers were not strong enough and the final failure was not significantly higher than the damage initiation point.

To improve the pseudo-ductility, a new series of tests has been completed by changing the high strain material from E-glass epoxy layers to S-glass epoxy with the same 913 resin. The proposed analytical approach was used and showed the potential to achieve promising pseudo-ductile responses while the yield stress was kept high. Since the aim of the study is to produce gradual failure, laminates with catastrophic failure were not tested and only four different layups of $[SG/C_n/SG]$ ($n = 1-3$) and $[SG_2/C_4/SG_2]$ with significant nonlinearity in their stress-strain curves were examined (SG stands for S-glass epoxy pre-impregnated layers).

The tensile specimens were made out of hybrid plates laid-up in a conventional way and cured for 60 min at 125 $^{\circ}$ C and 0.7 MPa. Cross-ply glass-epoxy end-tabs were bonded to the end of the cut specimens. Load was applied to the specimens under displacement control at 2 mm/min crosshead speed using a universal hydraulic test machine. The free length (not end tabbed) and the width of the specimens are 160 mm and 20 mm respectively and 5 specimens were tested for each layup. The overall thicknesses depend on the number of applied carbon and glass layers. Strains were measured using a video gauge system with a nominal 140 mm gauge length. The testing procedure of the second series is the same as the previous one and more details can be found in [13].

The material properties of E-glass, S-glass and TR30 carbon epoxy composites are given in Table 3. The interlaminar toughness

for the glass/carbon interface has been separately measured to be $G_{IIC} = 1.0$ N/mm using UD hybrid specimens with a single cut in the central carbon layer under tensile loading. In this type of test, delamination propagates stably and it is possible to work out the energy release rate from the stress level at which interlaminar cracks propagate [19,20]. Since the normal interlaminar stress around the crack tip is compressive when the specimen is in tension, the measured energy release rate is pure mode II [19].

The length and width of all specimens for prediction of high strain material failure (Eq. (32)) are assumed to be equal to $L = 160$ mm and $W = 20$ mm respectively. Although the value of the stress-concentration factor may vary in different specimens, such differences are not that large for different damage scenarios [21]. To keep the analysis simple and fast, the value of the stress concentration factor was assumed constant for all of the specimens, $K_t = 1.08$ based on the results given in [21,22]. It is possible to increase the accuracy of the stress-concentration factors, but this needs more sophisticated analyses and compromises the simplicity and low computational cost of the proposed method.

Since there is no direct method for measuring the average of the strength distribution of the UD layers, the 2.3% tensile strain at which the stress-strain curve of the $[EG_2/C/EG_2]$ layup with E-glass [13] deviates from the linear straight line is assumed as the average failure strain of the carbon epoxy layer and then multiplied by the modulus to find the average distribution strength. This gave a value of $\bar{S}_L = 2339$ MPa for the TR30 carbon composite, which is higher than the minimum strength given in Table 3. The latter is

Table 3

Material properties of E-glass, S-glass and TR30 carbon composites.

	E_t (GPa)	X_t (MPa)	Ply thickness (mm)	Weibull modulus
Hexcel E-Glass/913 [24]	38.7 [*]	1548 [†]	0.144	29.3
Hexcel S-Glass/913	45.7	2138 [†]	0.155	29.3 [‡]
SkyFlex TR30 carbon epoxy [25]	101.7	1962	0.030	–

^{*} Modified value for the measured thickness of glass layer.

[†] Calculated reference strength for unit volume.

[‡] Assumed equal to the Weibull modulus of E-glass/913 from [24].

more of a lower bound value, which is also affected by stress concentrations in the tests. The stiffness and strength of the S-glass epoxy composite has also been separately measured by testing pure UD S-glass epoxy composites.

Fig. 9 shows the predicted stress–strain curves (bold line) of the E-glass/TR30 carbon hybrids against the experimental results of the tested laminates from [13,14] (grey lines). The damage process of all of the laminates is well predicted and the stress–strain curves are in good agreement with the experiments. Both $[EG/C_m/EG]$ ($m = 1,2$) laminates have a catastrophic glass fibre failure which is well predicted by the proposed approach. The catastrophic delamination along with a load drop after first crack in the carbon layer of $[EG_2/C_n/EG_2]$ ($m = 3,4$) layups is also predicted very well. Initiation and saturation strain for carbon layer fragmentation in the $[EG_2/C/EG_2]$ layup is also in agreement with the obtained experimental results. Because an ideally uniform strength

distribution was assumed for the carbon layer, a constant load is predicted for fragmentation development.

The only significant difference between the analytical and experimental results is for the specimen $[EG_2/C_2/EG_2]$ in which, the failure stress and strain are overestimated. According to Fig. 9(d), fragmentation, diffuse delamination and final glass failure are all predicted at stress values very close to each other. This means that a small variation in the parameters may lead to a significant change in the predicted damage scenario. Fig. 10 shows the predicted response for the same laminate with similar material properties except the interlaminar toughness which was assumed $G_{IIC} = 1.01$ N/mm. A very small increment in G_{IIC} has led to change in the damage mode scenario and therefore a considerable change in the predicted stress–strain curve. Such a variation in the toughness may arise due to slight variation of the resin rich layer between the glass and carbon plies [23]. In fact, the experimental response for

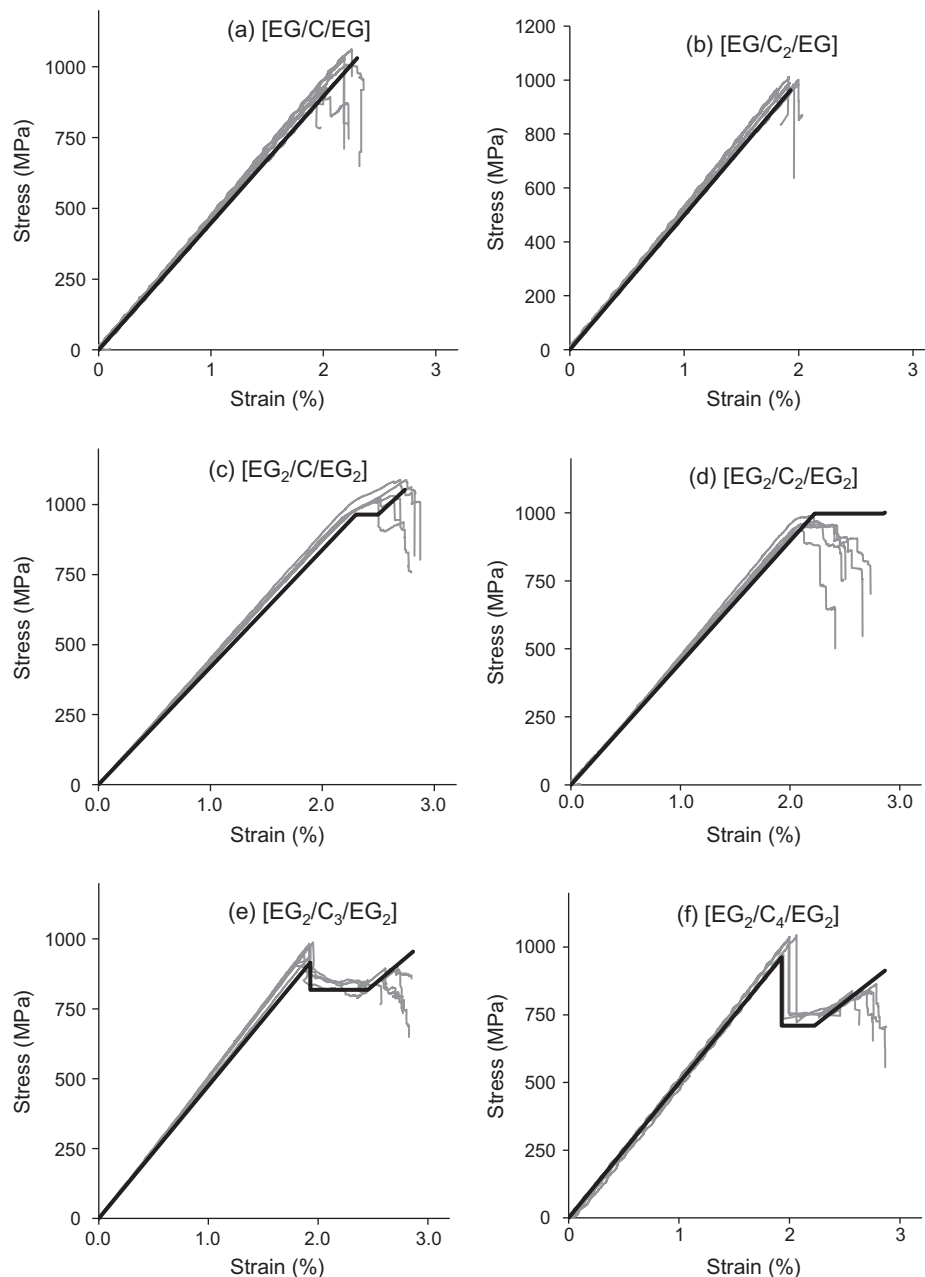


Fig. 9. Predicted stress–strain curve of E-glass/TR30 $[EG/C_m/EG]$ ($m = 1,2$) and $[EG_2/C_n/EG_2]$ ($n = 1-4$) laminates compared against experimental results.

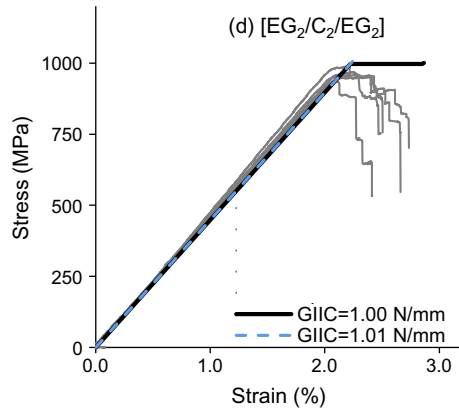


Fig. 10. The predicted stress–strain curve of $[EG_2/C_2/EG_2]$ with two different values of 1.00 and 1.01 N/mm for G_{IIIC} . (For interpretation of the references to colour in this figure legend, the reader is referred to the web version of this article.)

this laminate has certain similarities to both of the predicted responses in Figs. 9(d) and 10. Since the properties of real materials are not completely uniform over the whole specimen and there is always some variability in the constituents, it is very likely that the real damage process in this laminate is a mixture of both predicted damage scenarios shown in Figs. 9(d) and 10.

The new experimental stress–strain curves of the S-glass/TR30 hybrid are shown in Fig. 11. The best pseudo-ductile response without any load drop before final failure load is for the $[SG/C_2/$

SG] laminate with a failure strain of 3.4%. This response is a very good nonlinear stress–strain curve, significantly better than the $[EG_2/C_2/EG_2]$ laminate in terms of the obtained gradual failure and extra strain between initial damage and final failure.

The stress–strain curves of the S-glass/TR30 hybrid, shown in Fig. 11, are in a good agreement with the experimental results. The deviation from linearity in the experimental stress–strain curves of the $[SG/C/SG]$ layup shown in Fig. 11(a) is due to fragmentation of the TR30 carbon fibres. In the proposed analytical method, a uniform strength distribution is assumed for the low strain material (TR30 carbon epoxy). Therefore, the stress level is predicted to be constant during fragmentation, whereas the strength of fibres is not completely uniform in practice, which leads to the rising stresses during fragmentation. The predicted failure stress of the high strain material is 7% lower than the average experimental failure stress.

The $[SG/C_2/SG]$ laminate has two phases of gradual damage progression as shown in Fig. 11(b). The damage initiates with carbon ply fragmentation and this continues up to the saturation point. Dispersed delamination is the second damage mode in this layup and initiates from the cracks within the carbon layer (fragmentation). The final damage mode is glass fibre failure where the stress–strain curve terminates. Due to the dispersed fragmentation and delamination in this layup, the final failure strain is significantly higher than the carbon failure strain while there is no load drop until the final failure. The value of *pseudo-ductile strain*, the difference between the final failure strain and the strain on the initial slope line at the final failure stress, is equal to 1.0% which

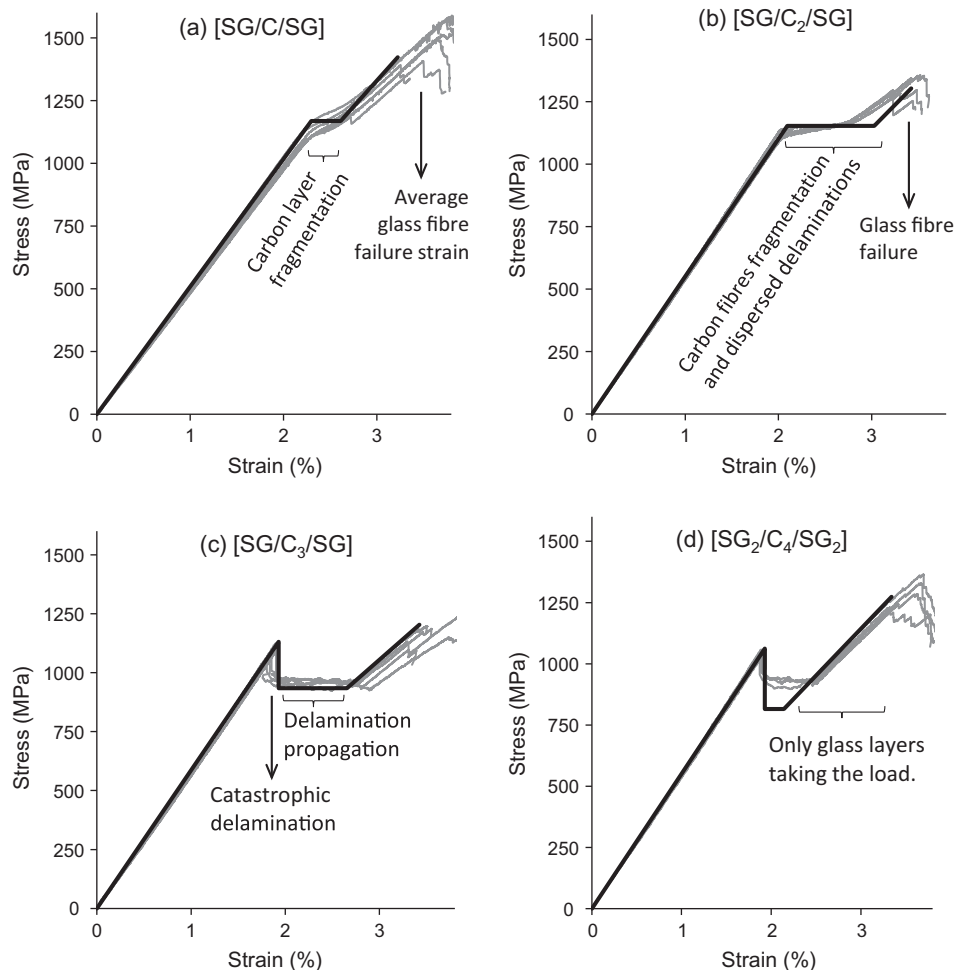


Fig. 11. Predicted stress–strain curves of $[G/C_m/G]$ ($m = 1-3$) and $[G_2/C_4/G_2]$ laminates made out of TR30/S-glass UD hybrid compared against experiments.

is 29% of final failure strain. This is a high pseudo-ductile response and has been achieved whilst maintaining the “yield” stress higher than 1140 MPa.

In both $[SG/C_3/SG]$ and $[SG_2/C_4/SG_2]$ layups, a catastrophic delamination propagates right after the first crack appears in the carbon layer. This catastrophic delamination introduces a significant load drop in the stress–strain curve and propagates stably to cover the whole glass/carbon interface. Therefore, there is no fragmentation in the carbon layer and the damage process is not uniformly dispersed over the whole specimen during delamination propagation. All of these different damage modes are predicted very well with the proposed analytical approach.

The predicted load drop in the $[SG_2/C_4/SG_2]$ laminate is bigger than what has been observed in Fig. 11(d) because a constant toughness value, $G_{IIc} = 1.0 \text{ N/mm}$, has been used for all different specimens. However, it has been reported [19,20] that an increase in the thickness of the laminate leads to higher values of interlaminar toughness. If a higher value of interlaminar toughness were applied in the $[SG_2/C_4/SG_2]$ laminate, the load drop after delamination would be lower and the stress level at which delamination propagates stably would be higher.

5. Conclusion

A new analytical approach for predicting the damage development in UD hybrid composites has been presented which is able to predict all possible combinations of damage modes in UD hybrids, making it possible to tailor the optimum desired response. This method was successful in predicting the damage process of different previously studied [13] and new hybrid composite specimens. The model is based on simple assumptions and runs very quickly, producing stress–strain responses that are in a good agreement with the experimental data.

Using the developed method, a new series of experiments with thin TR30 carbon/epoxy and standard thickness S-glass/epoxy layers have been performed. The best layup in this series was $[SG/C_2/SG]$ which produced 1.0% pseudo-ductile strain with a yield stress of more than 1130 MPa. Because of the well dispersed fragmentation and delamination along the specimens, no load drop was observed before final failure. This tensile response is a successful example of high performance pseudo-ductility achieved using commercially available constituents.

The proposed analytical approach is an ideal tool for further parametric studies. These can lead to a deeper understanding of the benefits and limitations of UD hybrid composites and enable the establishment of simple and accurate design guidelines which are crucial for an efficient design process. In the continuation of this work, the effect of different configurations and material combinations will be studied in a companion paper.

Acknowledgement

This work was funded under the UK EPSRC Programme Grant EP/I02946X/1 on High Performance Ductile Composite Technology in collaboration with Imperial College, London.

References

- [1] Bunsell AR, Harris B. Hybrid carbon and glass fibre composites. *Composites* 1974;5:157–64.
- [2] Aveston J, Kelly A. Tensile first cracking strain and strength of hybrid composites and laminates. *Philos Trans R Soc A Math Phys Eng Sci* 1980;294:519–34.
- [3] Aveston J, Cooper GA, Kelly A. Single and multiple fracture. In: *The Prop fibre Compos Conf Proceedings*, Natl Phys Lab. Guilford: IPC Science and Technology Press Ltd; 1971. p. 15–26.
- [4] Aveston J, Kelly A. Theory of multiple fracture of fibrous composites. *J Mater Sci* 1973;8:352–62.
- [5] Hayashi T, Koyama K, Yamazaki A, Kihira M. Development of new material properties by hybrid composition. *Fukugo Zair (Compos Mater)* 1972;1:18–20.
- [6] Manders PW, Bader MG. The strength of hybrid glass/carbon fibre composites. *J Mater Sci* 1981;16:2233–45.
- [7] Jones KD, DiBenedetto AT. Fiber fracture in hybrid composite. *Compos Sci Technol* 1994;51:53–62.
- [8] Zweben C. Tensile strength of hybrid composites. *J Mater Sci* 1977;12:1335–7.
- [9] Pitkeethly MJ, Bader MG. Failure modes of hybrid composites consisting of carbon fibre bundles dispersed in a glass fibre epoxy resin matrix. *J Phys D Appl Phys* 1987;20:315–22.
- [10] Swolfs Y, Crauwels L, Van Breda E, Gorbatiikh L, Hine P, Ward I, et al. Tensile behaviour of intralayer hybrid composites of carbon fibre and self-reinforced polypropylene. *Compos Part A Appl Sci Manuf* 2014;59:78–84.
- [11] Selmy AI, Elsesi AR, Azab NA, Abd El-baky MA. Monotonic properties of unidirectional glass fiber (U)/random glass fiber (R)/epoxy hybrid composites. *Mater Des* 2011;32:743–9.
- [12] Naito K, Yang J-M, Kagawa Y. Tensile properties of high strength polyacrylonitrile (PAN)-based and high modulus pitch-based hybrid carbon fibers-reinforced epoxy matrix composite. *J Mater Sci* 2011;47:2743–51.
- [13] Czel G, Wisnom MR. Demonstration of pseudo-ductility in high performance glass-epoxy composites by hybridisation with thin-ply carbon prepreg. *Compos Part A Appl Sci Manuf* 2013;52:23–30.
- [14] Jalalvand M, Czel G, Wisnom MR. Numerical modelling of the damage modes in UD thin carbon/glass hybrid laminates. *Compos Sci Technol* 2014;94:39–47.
- [15] Bakis CE, Nanni A, Terosky JA, Koehler SW. Self-monitoring, pseudo-ductile, hybrid FRP reinforcement rods for concrete applications. *Compos Sci Technol* 2001;61:815–23.
- [16] You Y-J, Park Y-H, Kim H-Y, Park J-S. Hybrid effect on tensile properties of FRP rods with various material compositions. *Compos Struct* 2007;80:117–22.
- [17] Harris HG, Somboson W, Ko FK. New ductile hybrid FRP reinforcing bar for concrete structures. *J Compos Constr* 1998;2:28–37.
- [18] Wisnom MR, Atkinson JW. Reduction in tensile and flexural strength of unidirectional glass fibre-epoxy with increasing specimen size. *Compos Struct* 1997;38:405–11.
- [19] Cui W, Wisnom MR, Jones M. An experimental and analytical study of delamination of unidirectional specimens with cut central plies. *J Reinf Plast Compos* 1994;13:722–39.
- [20] Czel G, Jalalvand M, Wisnom MR. Demonstration of pseudo-ductility in unidirectional hybrid composites incorporating carbon/epoxy platelets embedded in continuous glass/epoxy plies. *Compos Part A-Appl S*, submitted for publication.
- [21] Van den Heuvel PWJ, Goutianos S, Young RJ, Peijs T. Failure phenomena in fibre-reinforced composites. Part 6: a finite element study of stress concentrations in unidirectional carbon fibre-reinforced epoxy composites. *Compos Sci Technol* 2004;64:645–56.
- [22] Swolfs Y, Gorbatiikh L, Verpoest I. Stress concentrations in hybrid unidirectional fibre-reinforced composites with random fibre packings. *Compos Sci Technol* 2013;85:10–6.
- [23] Ji G, Ouyang Z, Li G. Effects of bondline thickness on mode-II interfacial laws of bonded laminated composite plate. *Int J Fract* 2010;168:197–207.
- [24] Hallett SR. Numerical investigation of progressive damage and the effect of layup in notched tensile tests. *J Compos Mater* 2005;40:1229–45.
- [25] Fuller J, Wisnom MR. Damage suppression in thin ply angle-ply carbon/epoxy laminates. In: *19th Int conf COMPOS Mater*, Montreal; 2013.